RERIC International Energy Journal: Vol. 15, No. 2, December 1993

An Investigation of the Effect of Dynamic Stall on Darrieus Turbines Applying the Cascade Model

Md. Maniruzzaman and Amalesh Chandra Mandal
Department of Mechanical Engineering
Bangladesh University of Engineering and Technology, Dhaka

ABSTRACT

A theoretical investigation of the effect of dynamic stall on straight-bladed Darrieus wind turbines is presented. To evaluate the effect of dynamic stall, empirical relations of aerodynamic characteristics are corporated into the cascade model. The overall and local experimental results are compared with the calculated values and it is observed that taking into consideration the dynamic stall phenomenon improves the prediction of local values.

INTRODUCTION

To predict the aerodynamic performance of Darrieus wind turbines, three categories of model are generally used: momentum model, vortex model and cascade model. Conventional momentum model [13] cannot predict the performance at very high solidity and high tip speed ratio because of the convergence problem, indicating the limitation of the theory. Vortex theory [14] also cannot reasonably predict the performance of Darrieus turbines as it often creates a convergence problem and takes very long computation time. But the cascade model which was introduced by Hirsch and Mandal [7] predicts the performance of Darrieus turbines reasonably well. It is based on the concepts of the cascade theory, similar to that used in turbomachines. However, there are certain phenomena, whose effects have not been incorporated into the model. One of the most important of these phenomena is dynamic stall.

When the angle of attack remains constant or varies slowly with time, the turbine encounters static stall. But when the angle of attack changes rapidly with time the turbine experiences dynamic stall. There are substantial differences between the characteristics of static and dynamic stall. Dynamic stall is a complex and unsteady flow phenomenon. Aerodynamic forces due to dynamic stall may be much higher than those due to static stall. As a result, when predicting the performance of Darrieus turbines, especially for local forces, there appear substantial differences between the experimental and calculated values.

With a view to incorporating the effect of dynamic stall, the Boeing-Vertol method [4] is introduced into the cascade model [7]. To simplify the analysis and eliminate certain deficiencies, some modification is carried out by introducing two empirical relations: one for lift characteristics in the prestall condition and another for the drag characteristics.

Two types of turbine blade sections NACA 0012 and NACA 0015 are included in the analysis. Two dimensional aerodynamic lift-drag characteristics for the prestall region are taken from the references [8,12,17].

SEMI-EMPIRICAL DYNAMIC STALL MODEL

Several experiments have been carried out in this field, but most of them are in relation to the helicopter rotor aerofoils [3,9]. The retreating side of these rotor aerofoils encounters a higher angle of attack, but in the advancing side, nominal angles are seen. Experiments show that loads on the aerofoil oscillating harmonically differ from those of non-pitching at the same angle of attack.

In the case of Darrieus turbines, as the turbine blade rotates, the local angle of attack changes continuously with time. At low tip speed ratio the angle of attack exceeds the stalling angle in most of the stations, thus the dynamic stalling effect needs to be incorporated into the analysis [5]. To include the effect of dynamic stall in the analysis, the Boeing-Vertol method [4] is applied to determine the lift characteristics.

In the Boeing-Vertol method, the blade angle is modified, the modified angle of attack α_m is determined from the following relation,

$$\alpha_m = \alpha - \gamma K_1 \left(\left| \frac{C_{\dot{\alpha}}}{2W} \right| \right) S_{\dot{\alpha}} \tag{1}$$

where α is the effective blade angle of attack, γ and K_1 are empirical constants, $\dot{\alpha}$ represents the instantaneous rate of change of α, $S_{\dot{\alpha}}$ is the sign of $\dot{\alpha}$ and W is the relative flow velocity.

This modified angle of attack is used to calculate the lift force coefficient due to the dynamic stalling effect in the following manner:

$$C_{ld} = \left(\frac{\alpha}{\alpha_m} \right) C_l \left(\alpha_m \right) \tag{2}$$

where $C_l (\alpha_m)$ is the lift value chosen corresponding to the modified angle of attack α_m and the value is taken from the two-dimensional lift characteristics with static stall conditions [8,12,17].

For low Mach numbers and for aerofoil thickness to chord ratios greater than 0.1, the value of γ is

$$\gamma = 1.4 - 6 \left(0.06 - t_c \right) \tag{3}$$

where t_c is the maximum airfoil thickness ratio. The K_1 value changes with the sign of the effective angle of attack, and this is determined from,

$$K_1 = 0.75 + 0.25 \times S_{\dot{\alpha}} \tag{4}$$

This formulation is applied when the angle of attack α is greater than the static stall angle or when the angle of attack is decreasing after having been above the stall angle. The Boeing-Vertol stall method is turned off when the angle of attack is below the stall angle and increasing.

Ham [5] introduced expressions for lift characteristics in the prestall region. In order to simplify the analysis and avoid some inconsistency in the prediction, a simple empirical relation for lift characteristics in prestall condition is introduced from the correlation of experimental results [6], which can be expressed as,

$$C_{lp} = C_l \left(1 + 0.03 \alpha \right) \tag{5}$$

In the analysis, to consider the effect of drag characteristics due to the dynamic stall, an empirical relation is introduced which can be written in the form,

$$C_{dd} = \frac{C_{ld}}{C_l(\alpha)} C_d(\alpha)(K) \tag{6}$$

where K is a factor. K is chosen as 1.0 in this expression.

The calculated drag values obtained from the equation (6) come closer to the calculated values presented by Cardona [1].

RESULTS AND DISCUSSIONS

Figures 1 to 3 depict the effect of dynamic stall on lift-drag characteristics of aerofoil blade section. From Fig. 1, it is observed that a large difference exists between the static lift characteristics and the experimental data presented by Ham et al. [6]. However, it is revealed from this figure that the present calculated lift characteristics including dynamic stall effect are closer to the experimental lift values. The primary characteristics of dynamic stall are its occurrence at an angle of attack greater than stall angle, followed by the shedding of vorticity from the leading and trailing edges.

Figure 2 shows the variation of the static lift [8,12,17] and the present calculated dynamic lift characteristics while Fig. 3 shows the variation of the static drag [8,12,17] and the present calculated dynamic drag characteristics. It can be seen from these figures that there occur remarkable variations of both lift and drag after the stalling angle. It occurs due to completely different flow phenomena in the case of the dynamic stalling condition [10].

In Fig. 1, the calculated values of the lift, including dynamic stall, are for the increasing angle of attack only, since the experimental values [6] are provided for the increasing angle of attack from 0° to 30°. However, in the Darrieus turbine during rotation of the blade, there occurs continuous increase and decrease of angle of attack. As a result, the calculated lift-drag values including dynamic stall, increase and decrease in comparison with the static values as shown in Figs. 2 and 3. The calculated values in Figs. 2 and 3 are presented as an example in order to reveal the nature of variation of dynamic lift-drag characteristics as the blade rotates in the turbine.

Figures 4 and 5 illustrate power coefficients vs. tip speed ratio of the present calculated values by applying the cascade model with and without dynamic stall and the experimental data of VUB wind tunnel test model [2]. The test was done at constant wind speed. At low tip speed ratio, no experimental data are available. At low tip speed ratio side, power coefficients become lower with dynamic stall than those without dynamic stall. Due to dynamic stall, lift value increases and so does the tangential force coefficient. But due to the increase of drag values, the tangential force coefficient decreases. The overall effect drops the value of the tangential force coefficient thereby decreasing the value of the power coefficient.

Figures 6 to 9 give comparisons of the present calculated values by applying the cascade model with and without dynamic stall and the experimental data from Sherbrooke University [16] at two different tip speed ratios 1.5 and 3.0, respectively. The available calculated values of the instantaneous forces by double multiple stream tube method with dynamic stall effect [11] are also plotted for comparison. Since the lift-drag characteristics of aerofoil NACA 0018 are not included in the program, for the present calculations lift-drag characteristics of aerofoil NACA 0015 are used. However, based on overall considerations, it may be concluded that the range of uncertainty

is of the order of 5% for using lift-drag characteristics of NACA 0015 in place of those of NACA 0018. It is seen from these figures that the present calculated values considering dynamic stall give a comparatively better correlation. For the non-dimensional normal forces, as Figs. 7 and 8 reveal, the correlation near the maximum peak value become excellent which is very important from the design point of view since the normal force coefficient affects the design of the turbine significantly. Considering the dynamic stall effect, both lift and drag coefficients increase. But the effects of lift on the tangential force coefficient is more prominent than that of drag. As a result, non-dimensional tangential forces increase. On the other hand, the normal force coefficient is influenced by the lift as well as by the drag. For this reason non-dimensional normal forces rise.

Present calculated blade forces by applying the cascade model with and without dynamic stall are compared with the experimental results of Sandia tow tank models [14] in Figs. 10 to 13. The comparisons are made at two different tip speed ratios, 2.5 and 5.0, respectively. Figures 10 and 11 show that at low tip speed ratio, the present calculated values of the instantaneous forces, taking into consideration dynamic stall, are improved in comparison to those where dynamic stall is not taken into consideration and closer to the experimental values. Results of non-dimensional tangential and normal forces at a tip speed ratio of 5.0 are shown in Figs. 12 and 13, respectively. The figures show improvements in the values of present calculated local force coefficients with dynamic stalling.

In Figs. 12 and 13 calculated values of forces by the quasi-steady vortex model [15] are also plotted. The present calculated force coefficients with dynamic stall show better agreement with the experimental values than those by the quasi-steady vortex model.

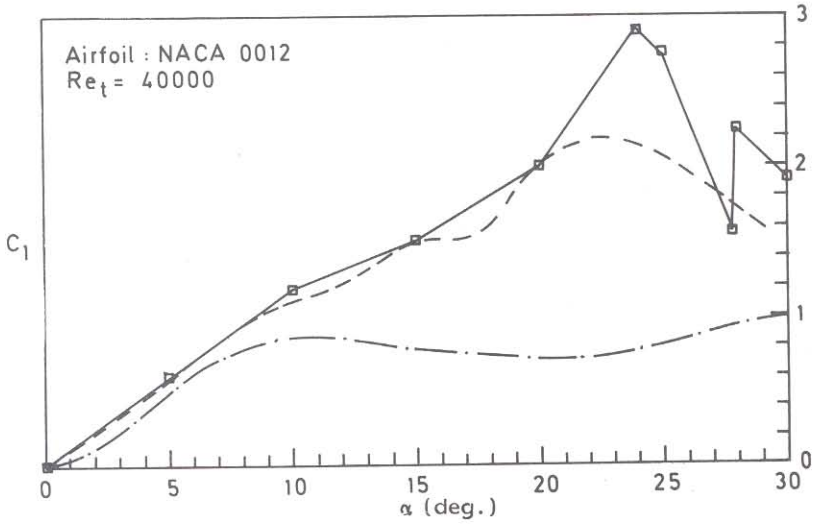

Fig. 1. Comparisons of calculated and experimental lift characteristics.

—·—·—·— static lift [Refs. 8, 12, 17]
— — — — calc. dynamic lift [present]
—□—□—□— experimental lift [Ref. 6]

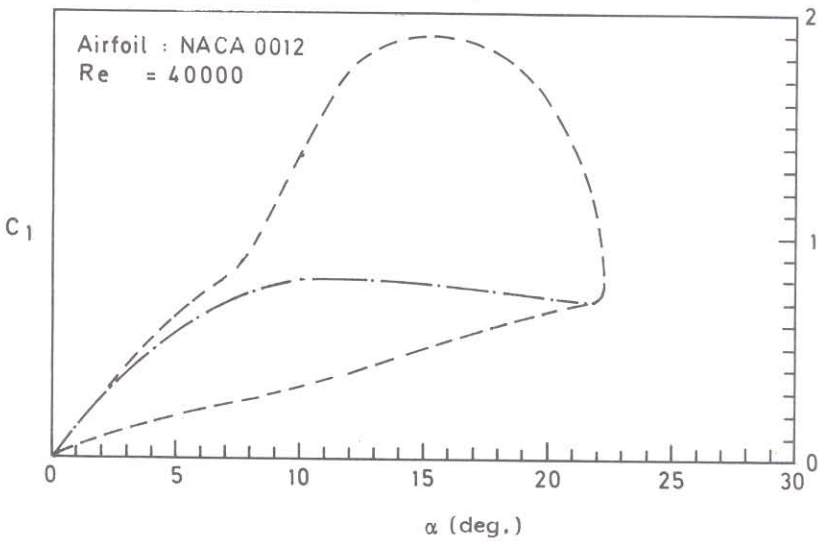

Fig. 2. Variation of lift characteristics for static and dynamic stall conditions.

—·—·—·— static lift [Refs. 8, 12, 17]
— — — — calc. dynamic lift [present]

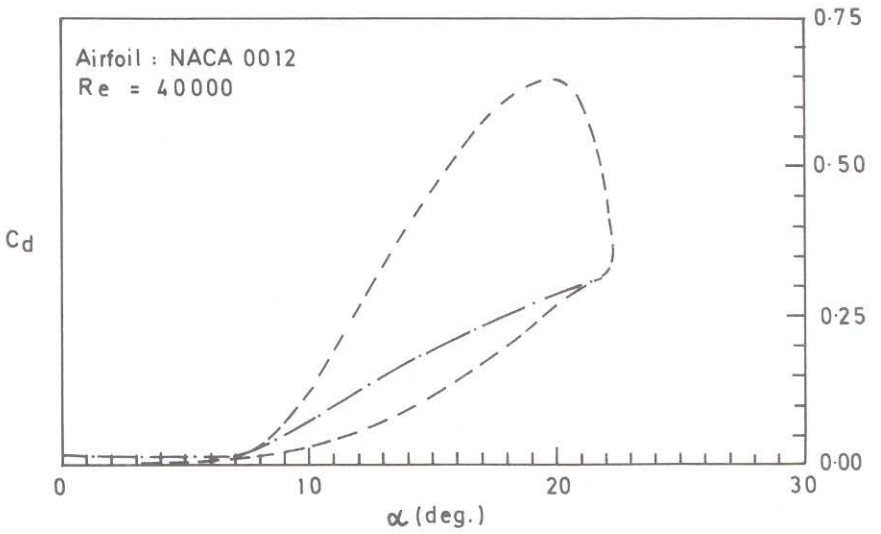

Fig. 3. Variation of drag characteristics for static and dynamic stall conditions.

—·—·—·— static drag [Refs. 8, 12, 17]
— — — — calc. dynamic drag [present]

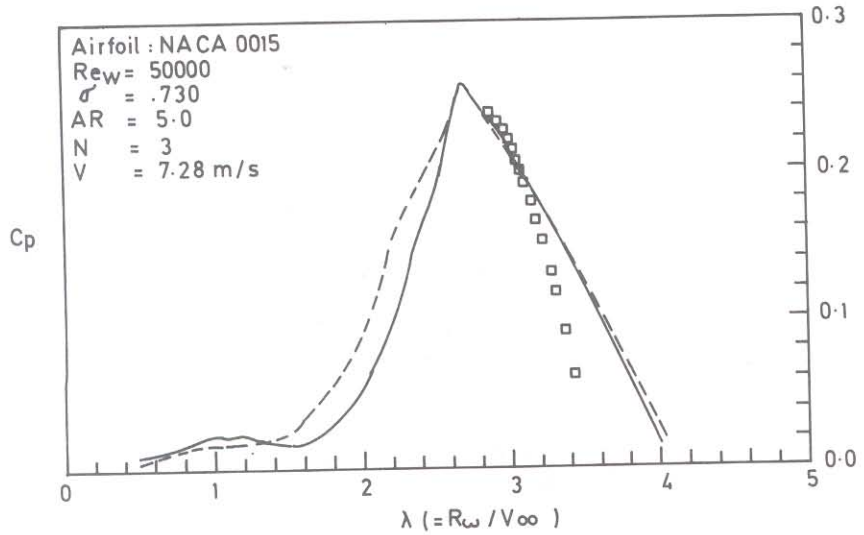

Fig. 4. Comparisons of experimental and calculated overall power coefficients.

— — — — calc. (cascade model without dynamic stall) [present]
——————— calc. (cascade model with dynamic stall) [present]
□ □ □ expt. (VUB-model) [Ref. 2]

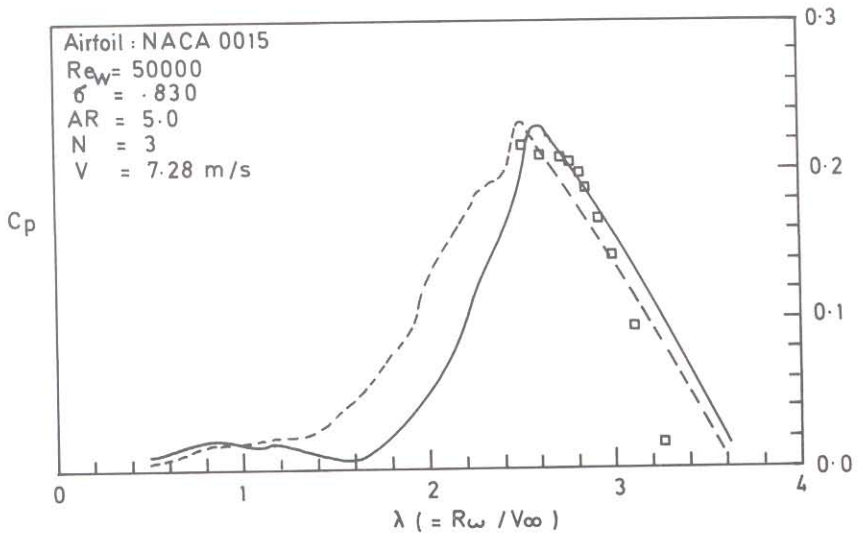

Fig. 5. Comparisons of experimental and calculated overall power coefficients.

— — — — calc. (cascade model without dynamic stall) [present]
——————— calc. (cascade model with dynamic stall) [present]
□ □ □ expt. (VUB-model) [Ref. 2]

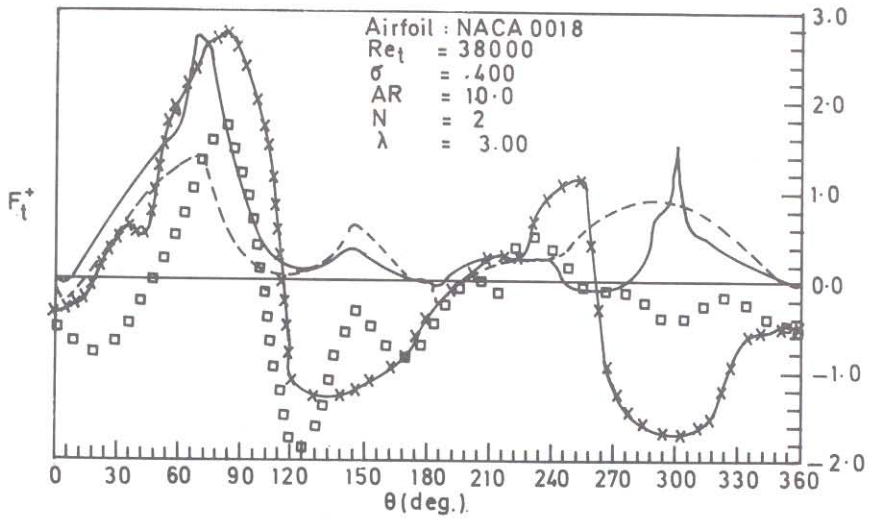

Fig. 6. Comparisons of experimental and calculated non-dimensional tangential forces.

— — — — calc. (cascade model without dynamic stall) [present]
——— calc. (cascade model with dynamic stall) [present]
—×—×—×— calc. (double multiple streamtube with dynamic stall) [Ref. 11]
□ □ □ expt. (Sherbrooke) [Ref. 16]

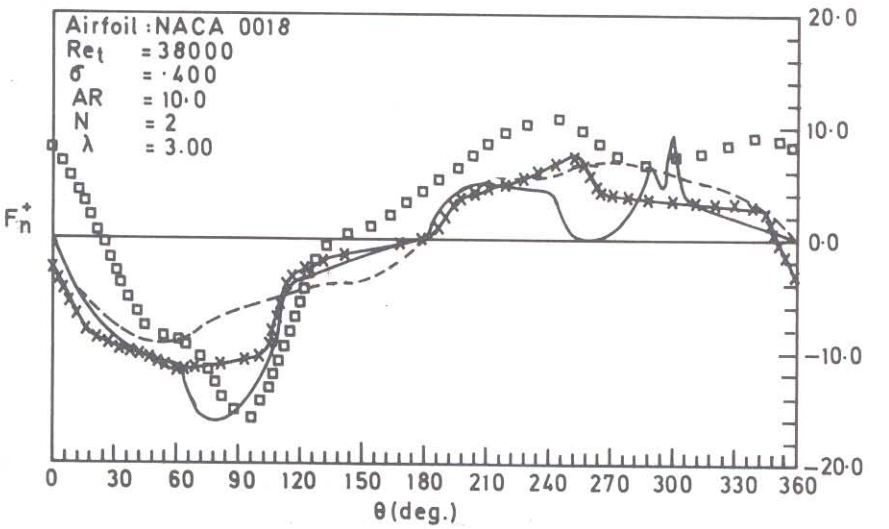

Fig. 7. Comparisons of experimental and calculated non-dimensional normal forces.

— — — — calc. (cascade model without dynamic stall) [present]
——— calc. (cascade model with dynamic stall) [present]
—×—×—×— calc. (double multiple streamtube with dynamic stall) [Ref. 11]
□ □ □ expt. (Sherbrooke) [Ref. 16]

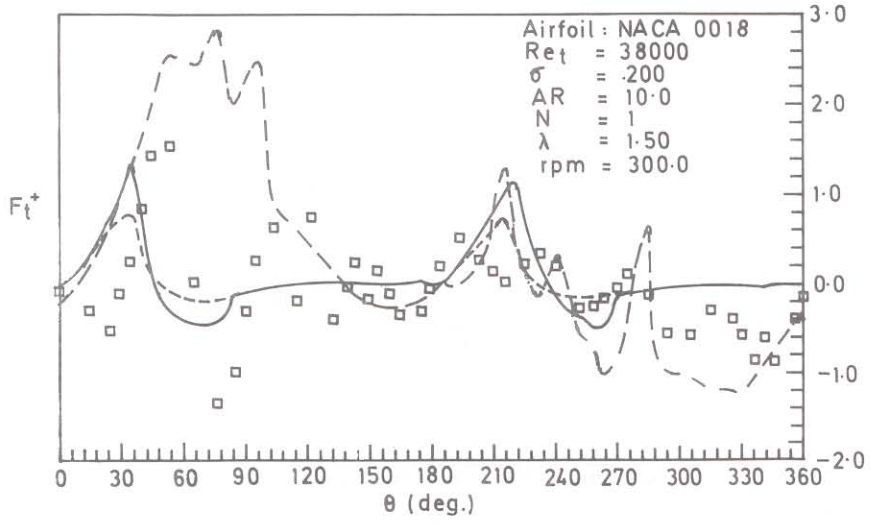

Fig. 8. Comparisons of experimental and calculated non-dimensional tangential forces.

- - - - - - - calc. (cascade model without dynamic stall) [present]
——————— calc. (cascade model with dynamic stall) [present]
— — — — calc. (double multiple streamtube with dynamic stall) [Ref. 11]
□ □ □ expt. (Sherbrooke) [Ref. 16]

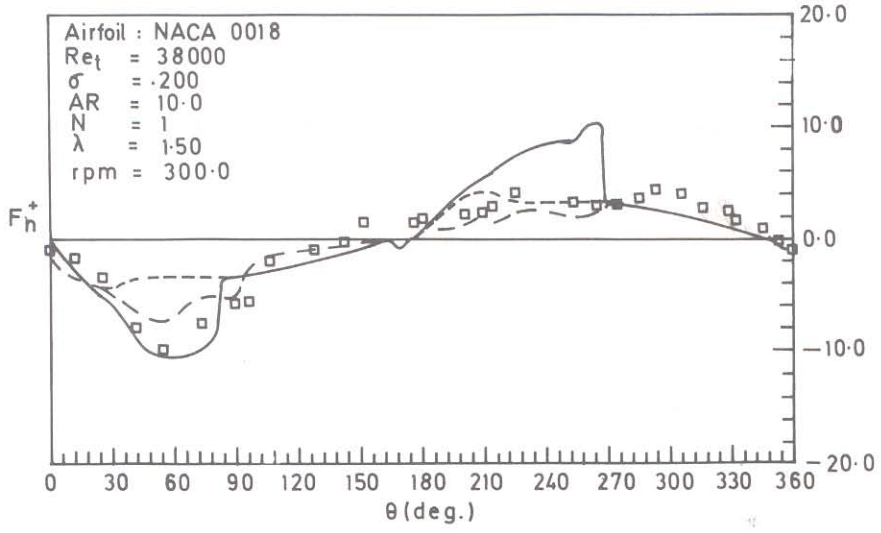

Fig. 9. Comparisons of experimental and calculated non-dimensional normal forces.

- - - - - - - calc. (cascade model without dynamic stall) [present]
——————— calc. (cascade model with dynamic stall) [present]
— — — — calc. (double multiple streamtube with dynamic stall) [Ref. 11]
□ □ □ expt. (Sherbrooke) [Ref. 16]

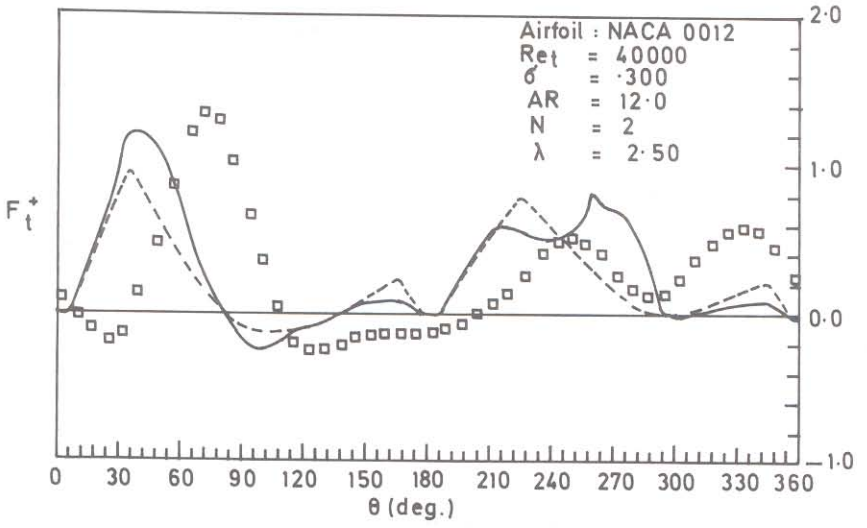

Fig. 10. Comparisons of experimental and calculated non-dimensional tangential forces.

— — — — calc. (cascade model without dynamic stall) [present]
——— calc. (cascade model with dynamic stall) [present]
□ □ □ expt. (Sandia) [Ref. 14]

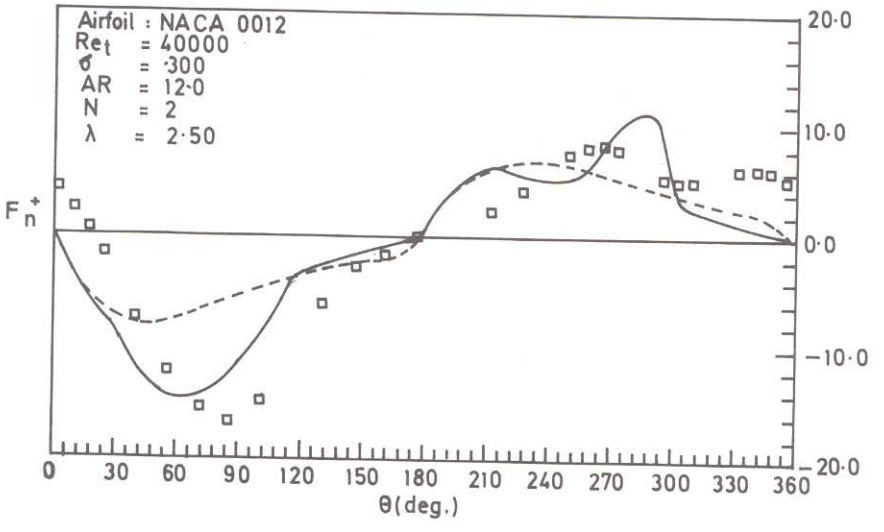

Fig. 11. Comparisons of experimental and calculated non-dimensional normal forces.

— — — — calc. (cascade model without dynamic stall) [present]
——— calc. (cascade model with dynamic stall) [present]
□ □ □ expt. (Sandia) [Ref. 14]

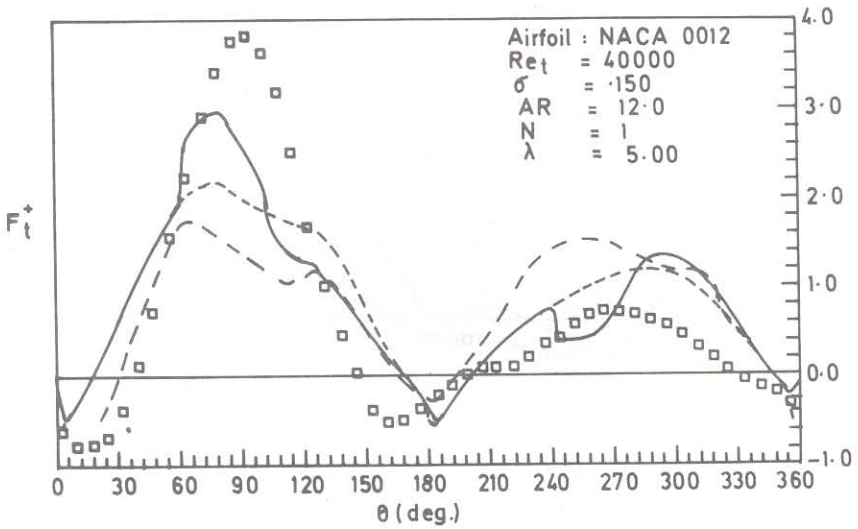

Fig. 12. Comparisons of experimental and calculated non-dimensional tangential forces.

- calc. (cascade model without dynamic stall) [present]
- calc. (cascade model with dynamic stall) [present]
- calc. (quasi-steady vortex model) [Ref. 15]
- expt. (Sandia) [Ref. 14]

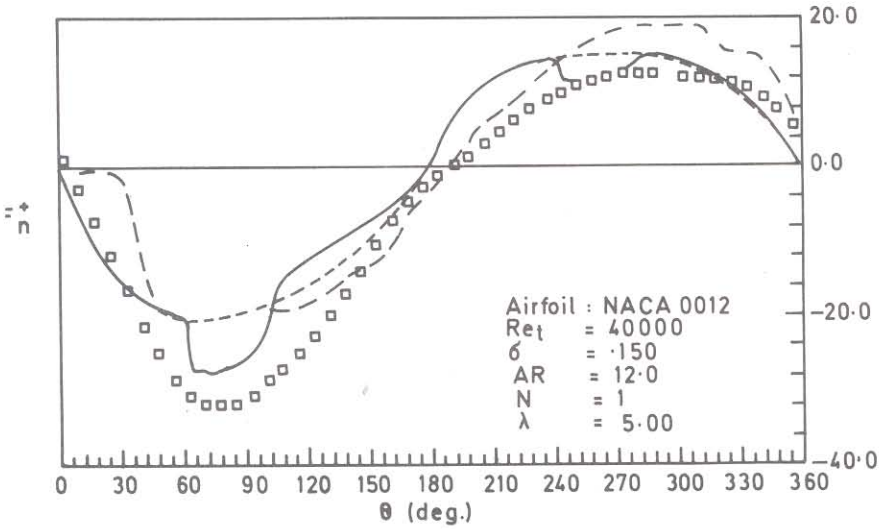

Fig. 13. Comparisons of experimental and calculated non-dimensional normal forces.

- calc. (cascade model without dynamic stall) [present]
- calc. (cascade model with dynamic stall) [present]
- calc. (quasi-steady vortex model) [Ref. 15]
- expt. (Sandia) [Ref. 14]

CONCLUSIONS

Including the effect of dynamic stall with the cascade theory, the overall values of power coefficients are changed negligibly at the higher tip speed ratios while they are changed appreciably at the lower tip speed ratios.

The correlation of the calculated and the experimental results shows that the calculated local values by cascade theory including dynamic stall effect, become relatively closer to the experimental values in comparison with those obtained by applying other models.

Maximum peak force coefficient is very important in the stress analysis of Darrieus turbine blades. The present analysis shows a good correlation between the value of maximum peak normal force coefficient and the experimental results.

At the present moment sufficient experimental data are not available to check the expressions of lift-drag characteristics including dynamic stalling effect. These are necessary to make further comparisons.

NOMENCLATURE

A	projected frontal area of turbine
AR	aspect ratio $= H / C$
C	blade chord
C_d	blade drag coefficient
C_{dd}	blade drag coefficient due to dynamic stall effect
C_l	blade lift coefficient
C_{lp}	lift coefficient for prestall condition
C_{ld}	blade lift coefficient due to dynamic stall effect
C_n	normal force coefficient
C_p	turbine overall power coefficient $= \dfrac{P_o}{\frac{1}{2}\rho A V_\infty^3}$
C_t	tangential force coefficient
F_n^+	non-dimensional normal force $= C_n \left(\dfrac{W}{V_\infty}\right)^2$
F_t^+	non-dimensional tangential force $= C_t \left(\dfrac{W}{V_\infty}\right)^2$
H	height of the turbine
K	factor to include dynamic stall in drag value
K_1	an empirical constant
N	number of blades
P_o	overall power

rpm turbine speed in revolutions per minute

R turbine radius

Re_t turbine speed Reynolds number = $\frac{R\,\omega\,C}{\nu}$

Re_w wind speed Reynolds number = $\frac{V_\infty\,C}{\nu}$

S_α sign of rate of change of angle of attack

t_c maximum blade thickness as a fraction of chord

V local velocity

V_∞ wind velocity

W relative flow velocity

α angle of attack

α_m modified angle of attack for dynamic stall effect

γ an empirical constant

θ azimuth angle

λ tip speed ratio = $\frac{R\,\omega}{V_\infty}$

ν kinematic viscosity

ρ fluid density

σ solidity = $\frac{NC}{R}$

ω angular velocity of turbine in rad/sec

REFERENCES

1. Cardona, J.L. (1984), Flow Curvature and Dynamic Stall Simulated with an Aerodynamic Free-Vortex Model for VAWT, *Wind Engineering*, Vol. 8, No. 3, pp.135-143.
2. Decleyre, W., D.V. Aerschot and Ir. CH. Hirsch (1981), The Effects of Reynolds Number on the Performance Characteristics of Darrieus Windmills with Troposkien and Straight-Blades, *Proceedings of the International Colloquium on Wind Energy*, Brighton, August, pp.243-248.
3. Ericsson, L.E. and J.P. Reding (1978), Engineering Analysis of Dynamic Stall, *Proceeding of the ASME Winter Annual Meeting*, San Francisco, Calif., December, pp.117-123.
4. Gormont, R.E. (1973), *A Mathematical Model of Unsteady Aerodynamics and Radial Flow for Application to Helicopter Rotors*, U.S. Army Air Mobility R & D Laboratory, Vertol Division, Philadelphia, Pa., Report on Boeing-Vertol Contract DAAJOV-71-c-0045, May.
5. Ham, N.D. (1968), Aerodynamic Loading on a Two-dimensional Airfoil during Dynamic Stall, *Journal of the AIAA*, Vol. 6, No. 10, October.

6. Ham, N.D. and M.S. Garelick (1968), Dynamic Stall Considerations in Helicopter Rotor, *Journal of the American Helicopter Society*, Vol. 13, No. 2, April.
7. Hirsch, Ir. CH. and A.C. Mandal (1987), A Cascade Theory for the Aerodynamic Performance of Darrieus Turbines, *Wind Engineering*, Vol. 11, No. 3.
8. Jacob, E.N. and A. Sherman (1937), *Airfoil Section Characteristics as Affected by Variations of the Reynolds Number*, NACA-TR-586, September.
9. Mc Croskey, J.W. and L.S. Pucci (1982),Viscous-Inviscid Interaction on Oscillating Airfoils in Subsonic Flow, *AIAA Journal*,Vol. 20, Feb., pp.167-174.
10. Mehta, U.B. (1977), Dynamic Stall on an Oscillating Airfoil, *Proceedings of AGARD Fluid Dynamics Panel Symposium on Unsteady Aerodynamics*, AGARD CPP-227, September.
11. Paraschivoiu, I. (1983), Predicted and Experimental Aerodynamic Forces on the Darrieus Rotor, *Journal of Energy*, Vol. 7, No. 6, Nov.-Dec., pp.610-615.
12. Sheldahl, R.E. and B.F. Blackwell (1976), Aerodynamic Characteristics of Four Symmetrical Aerofoil Sections Through 180 Degrees Angle of Attack at Low Reynolds Number, *Vertical-Axis Wind Turbine Technology Workshop*, May 17-20.
13. Strickland, J.H. (1975), *The Darrieus Turbine : A Performance Prediction Model Using Multiple Steamtubes*, Sandia Laboratories Report, SAND 75-0431, October.
14. Strickland, J.H., T. Smith and K. Sun (1981), *A Vortex Model of the Darrieus Turbine: An Analytical and Experimental Study*, Sandia Laboratories Report, SAND 81-7017, June.
15. Strickland, J.H., B.T. Webster and T. Nguyen (1979), A Vortex Model of the Darrieus Turbine: An Analytical and Experimental Study, *Journal of Fluids Engineering*, Vol. 101, No. 4, Dec., pp.500-505.
16. Vittecoq, P. and A. Laneville (1982), *Etude en Soufferie d'un Rotor du Type Darrieus*, Mechanical Engineering Department, University of Sherbrooke, Canada, Report ME-82-2, August.
17. Willmer, A.C. (1979), Low Reynolds Number Tests on the NACA 0015 Section, *1st BWEA Workshop*, April.